AIAA JOURNAL
Vol. 47, No. 3, March 2009

Nonlinear Control of a Membrane Mirror Strip Actuated Axially and in Bending

Jamil M. Renno* and Daniel J. Inman†
Virginia Polytechnic Institute and State University, Blacksburg, Virginia 24061-0261
and
Konda Reddy Chevva‡
California Institute of Technology, Pasadena, California 91125-8100

DOI: 10.2514/1.31166

The sliding mode technique is used to control the deformation of a membrane mirror strip augmented with two macrofiber composite bimorphs located near the ends of the strip. The first bimorph is actuated in bending and the second is actuated axially. The structure is modeled as an Euler–Bernoulli beam under tensile load and the macrofiber composite patches are modeled as monolithic piezoceramic wafers. To cast the system into a finite-dimensional state-space form, the finite element method is used, and the model presented accounts for the dynamics of the augmented bimorphs. The membrane strip is placed under uniform tension. Because one of the bimorphs acts axially, the resulting tension in the membrane strip is discontinuous at the location of this bimorph and, consequently, the obtained model is nonlinear. First, we validate the model experimentally by considering the system in its quasi-linear state, then we consider the control problem. We formulate the regulation problem by using the sliding mode technique. Additionally, to allow coupling this system with an adaptive optics scheme, the shape-control problem is considered as well. The control law uses both actuators: the bending and axial bimorphs. However, a system singularity dictates using a switching command to avoid this singularity. Various examples are presented for the regulation and shape-control problems. The simulation results demonstrate the efficacy of the proposed control law.

Nomenclature

$\boldsymbol{B}_1$	=	input vector of the bending bimporph
b	=	width, m
$\boldsymbol{C}$	=	damping matrix
c	=	structural damping, N.s/m^2
d_{31}	=	piezoelectric coupling coefficient in the {31} mode, m/V
E	=	Young's modulus of elasticity, N/m^2
f_{exp}	=	natural frequency obtained through experiment, Hz
f_{FEM}	=	natural frequency obtained through the finite element method, Hz
h	=	thickness, m
$\boldsymbol{K}$	=	stiffness matrix
L	=	length of the membrane strip, m
$\boldsymbol{M}$	=	mass matrix
N	=	number of discretized elements presenting the structure
$\mathcal{T}$	=	uniform tensile load along the structure, N
t	=	time, s
w	=	transverse deflection, m
x	=	coordinate along strip, m
γ	=	air-damping coefficient, N $\cdot$ s/m^2
ρ	=	mass density, kg/m^3
τ	=	tension in the strip, N
ϕ	=	B-spline test function

Subscripts

i, j	=	variable number
k	=	property of, or input to the kth bimorph ($k = 1, 2$)
m	=	membrane property

Received 20 March 2007; revision received 15 September 2008; accepted for publication 11 October 2008.

*Graduate Student, Center for Intelligent Material Systems and Structures. Student Member AIAA.

†G. R. Goodson Professor and Director, Center for Intelligent Material Systems and Structures; dinman@vt.edu. Fellow AIAA (Corresponding Author).

‡Postdoctoral Researcher, Control and Dynamical Systems; currently Research Engineer, United Technologies Research Center, East Hartford, CT 06108. Member AIAA.

I. Introduction

FUTURE space-based telescopes will use large membrane mirrors as their optical surfaces. Membrane mirrors are lightweight; they can be compactly stored, and they have the potential to provide high-quality optical imaging. The U.S. Air Force Research Laboratory began a program of research on membrane technologies in 1995. Various government organizations, including the U.S. Air Force, the U.S. Department of Defense, and NASA agencies such as the Jet Propulsion Laboratory have a mounting interest in this area. The goal is to develop, launch, and optically control membrane mirrors for military and civilian applications.

In this paper, we consider the control of an in-plane piezoelectrically actuated membrane mirror strip with actuators acting axially and in bending. The underlying idea of this research effort is to augment an appropriate number of actuators along the outer rim of a membrane mirror and use their control authority to correct for optical aberrations. As a prelude for studying the two-dimensional structure, we investigate the control problem of a membrane mirror strip with axial and bending in-plane piezoelectric actuators.

Research in the field of large lightweight space structures has been ongoing since the 1960s. There are many review articles that present recent developments in this area [1–4]. Also, a two-volume series edited by Jenkins [5,6] provides a comprehensive coverage of this technology, including topics ranging from the mechanics of membranes to inflatable space habitats. More specifically, research of membrane mirrors has received considerable attention. Many researchers discussed modeling, control, and experimental challenges in the area of membrane mirrors [7–11]. However, the ultimate objective of research in the area of membrane mirrors remains to correct for optical aberrations. The study of optical aberrations is a separate and well-developed area in its own right. Researchers have proposed boundary displacement to achieve

optical correction [12–14]. For example, Wilkes et al. [15] prestrained the membrane and then used boundary control to correct for aspheric aberrations. Other researchers used in-plane actuation, such as Shepherd et al. [16,17], who presented the construction and testing of a 5 in. membrane mirror actuated in-plane using piezoelectric elements. They implemented a control algorithm developed from the results of a finite element model to achieve quasi-static shaping of the mirror. Ruggiero [18] presented a basis for conversing between the optical mode shapes and mechanical mode shapes. Optical aberrations of an incoming wave front to circular mirror are usually described as a linear combination of optical mode shapes (Zernike polynomials), and the mechanical deformations of a circular membrane are described as a linear combination of mechanical mode shapes (Bessel functions). The ability to induce certain mode shapes of the circular membrane would ultimately give the ability to correct for optical aberrations through the mapping existing between the optical and mechanical mode shapes.

In the preceding literature survey, in-plane actuators (bimorphs or unimorphs) were used to actuate the membrane mirror in bending only. Axial actuation has not been previously investigated in the literature. To this end, the goal of our research is to model and control a membrane mirror augmented with smart actuators around its outer rim. The actuators can act axially or in bending. As a prelude to studying a two-dimensional membrane, we focus on a membrane strip augmented with two microfiber composite (MFC) bimorphs near its ends. Wilkie et al. [19] presented the design, manufacturing, and testing of MFCs. These actuators use interdigitated electrodes for poling and subsequent actuation of an internal layer of machined piezoceramic fiber, which makes them lighter than a piezoceramic actuator of the same size.

Recently, Renno et al. [20] modeled a strip of membrane mirror augmented with a single piezoelectric bimorph. The model of [20] improves the model presented in [18] for the same structure by accounting for the added mass and flexural rigidity of the piezoelectric bimorph. Renno and Inman [21] presented an experimentally validated model for a membrane mirror strip augmented with multiple MFC actuators acting in bending as well.

To this end, this paper treats the control of a membrane mirror strip augmented with two MFC bimorphs. One of the bimorphs acts in bending (BBM), whereas the other acts axially (ABM). The presence of the ABM renders this system nonlinear. The structure was treated as a quasi-linear system by Renno and Inman [21] and the model was validated experimentally.

In this paper, we propose using bending and axial actuation to control the transverse motion of a membrane mirror strip. We derive a sliding mode controller to regulate the system. We also treat the shape-control problem, which will enable coupling this system with an adaptive optics scheme. The controller uses both actuators, BBM and ABM. A switching command is used as well to avoid system singularities. The simulation results presented show that the controller satisfactorily suppresses the vibration of the membrane strip in the presence of system uncertainties and can achieve shape control as well.

The remaining of this paper is organized as follows. Section II presents the dynamic model of the structure and the formulation of the problem. A sample membrane strip was experimentally tested using laser vibrometry techniques. The experimental setup and results are described in Sec. III. In Sec. IV, a sliding mode controller is derived in the presence of system uncertainties. A case study is presented in Sec. V, along with simulation results of the regulation and tracking problems. Finally, conclusions for this work are drawn in Sec. VI.

II. Dynamic Model and Problem Formulation

The model of a membrane strip augmented with two MFC bimorphs was presented in [21]. Figure 1 shows a schematic of the structure under study. The gravity field is perpendicular to the x–w plane. The membrane strip is augmented with two MFC bimorphs, ABM and BBM, which act axially and in bending, respectively. The structure is modeled as an Euler–Bernoulli beam under tension and

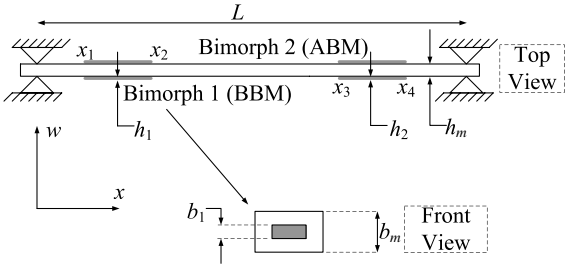

Fig. 1 Schematic of a membrane strip with two piezoelectric bimorphs near its ends.

its transverse motion is governed by

$$\rho_A(x)\frac{\partial^2 w(x,t)}{\partial t^2}+\frac{\partial^2 M_x(x,t)}{\partial x^2}-\frac{\partial}{\partial x}\left(\tau(x,t)\frac{\partial w(x,t)}{\partial x}\right)+\gamma\frac{\partial w(x,t)}{\partial t}=-\frac{\partial^2[M_x(x,t)]_1}{\partial x^2} \tag{1}$$

where $\rho_A(x)$ and $M_x(x,t)$ are the linear density and internal bending moment of the structure (see the Appendix). Moreover, $[M_x(x,t)]_1$ is the bending moment induced by the BBM. Because the membrane strip cannot resist a bending moment at its boundaries, the boundary conditions are pinned–pinned. The linear density, flexural stiffness, and structural damping of the structure are nonuniform due to the bimorphs, and hence the finite element method (FEM) is used to cast Eq. (1) in a finite-dimensional form. Cubic B-splines are used to span the finite element space of the structure, constituting a set of linearly independent functions that form a basis for the finite element approximation, [22]. The interested reader is advised to consult [23] for more information about B-splines. Hollig [24] also presented several types of B-spline basis for approximation and boundary-value problems. The finite-dimensional equations of the structure are

$$\begin{Bmatrix}\dot{\bar{\boldsymbol{w}}}\\ \dot{\bar{\boldsymbol{v}}}\end{Bmatrix}=\begin{bmatrix}\boldsymbol{0}_{N\times N} & \boldsymbol{I}_{N\times N}\\ -\boldsymbol{M}^{-1}\boldsymbol{K} & -\boldsymbol{M}^{-1}\boldsymbol{C}\end{bmatrix}\begin{Bmatrix}\bar{\boldsymbol{w}}\\ \bar{\boldsymbol{w}}\end{Bmatrix}+\begin{bmatrix}\boldsymbol{0}_{N\times 1}\\ \boldsymbol{M}^{-1}\boldsymbol{B}_1\end{bmatrix}V_1(t) \tag{2}$$

where $\bar{\boldsymbol{w}}$ is the deflection vector, $\bar{\boldsymbol{v}}$ is the velocity vector, and $V_1(t)$ is the voltage applied to the BBM. The dot indicates the derivative with respect to time. The system matrices are given as

$$\begin{aligned}\boldsymbol{M}&=\left[\int_0^L \rho_A(x)\phi_i(x)\phi_j(x)\mathrm{d}x\right]_{(i,j=1,\ldots,N)}\\ \boldsymbol{B}_1&=\left[2(\kappa_B)_1\int_0^L \chi_1(x)\phi_j''(x)\mathrm{d}x\right]_{(j=1,\ldots,N)}\\ \boldsymbol{K}&=\left[\int_0^L (EI(x)\phi_i''(x)\phi_j''(x)+\tau(x,t)\phi_i'(x)\phi_j'(x))\mathrm{d}x\right]_{(i,j=1,\ldots,N)}\\ \boldsymbol{C}&=\left[\int_0^L (cI(x)\phi_i''(x)\phi_j''(x)+\gamma\phi_i(x)\phi_j(x))\mathrm{d}x\right]_{(i,j=1,\ldots,N)}\end{aligned} \tag{3}$$

where the prime indicates the spatial derivative, and the expressions for $EI(x)$ and $cI(x)$ are given in the Appendix. The presence of the ABM causes the tension to be discontinuous:

$$\tau(x,t)=\mathcal{T}+2(\kappa_A)_2 S_{3,4}\chi_2(x)V_2(t) \tag{4}$$

where $V_2(t)$ is the voltage applied at the ABM. The spatial function $\chi_k(x)$ and the bending constant of the BBM and the axial constant of the ABM [$(\kappa_B)_1$ and $(\kappa_A)_2$, respectively] are given in the Appendix. The spatial function $\chi_k(x)$ marks the location of the kth bimorph, and $S_{3,4}(x)$ is an indicator function stating that opposite but equal strains develop about the midpoint of the ABM:

$$S_{3,4}(x)=\begin{cases}1 & \text{if } x<(x_3+x_4)/2\\ 0 & \text{if } x=(x_3+x_4)/2\\ -1 & \text{if } x>(x_3+x_4)/2\end{cases} \tag{5}$$

Table 1 Properties of the Kapton strip and MFC patch

Property	Kapton strip	MFC patch
Density, kg/m^3	1420	994
Width, cm	2.5	2.5
Thickness, mm	51×10^{-3}	0.3
Length, cm	22	3.8
Young's modulus, GPa	3	34.5
Air-damping coefficient, N $\cdot$ s/m^2	0.02	0.02
Kelvin–Voigt coefficient, N $\cdot$ s/m^2	5.2495×10^5	2.5536×10^3
Piezoelectric coupling coefficient, pm/V	——	−210

Substituting the expression for the tension from Eq. (4) in the stiffness matrix $\boldsymbol{K}$ yields

$$\boldsymbol{K} = \left[\int_0^L (EI(x)\phi_i''(x)\phi_j''(x) + [\mathcal{T} + 2(\kappa_A)_2 S_{3,4}(x)\chi_2(x)V_2(t)]\phi_i'(x)\phi_j'(x))\mathrm{d}x \right]_{(i,j=1,\ldots,N)} \tag{6}$$

For a constant voltage $V_2(t)$, the stiffness matrix would be constant. Then Eq. (2) becomes linear, albeit in the quasi sense. The stiffness matrix would then be

$$\boldsymbol{K} = \boldsymbol{K}_1 + \boldsymbol{K}_2 V_2(t) \tag{7}$$

where

$$\boldsymbol{K}_1 = \left[\int_0^L (EI(x)\phi_i''(x)\phi_j''(x) + \mathcal{T}\phi_i'(x)\phi_j'(x))\mathrm{d}x \right]_{(i,j=1,\ldots,N)}$$
$$\boldsymbol{K}_2 = 2(\kappa_A)_2 \left[\int_0^L S_{3,4}(x)\chi_2(x)\phi_i'(x)\phi_j'(x)\mathrm{d}x \right]_{(i,j=1,\ldots,N)} \tag{8}$$

Now Eq. (2) can be rearranged into the standard state-space form as

$$\begin{Bmatrix} \dot{\bar{w}} \\ \dot{\bar{v}} \end{Bmatrix} = \begin{bmatrix} \boldsymbol{0}_{N\times N} & \boldsymbol{I}_{N\times N} \\ -\boldsymbol{M}^{-1}\boldsymbol{K}_1 & -\boldsymbol{M}^{-1}\boldsymbol{C} \end{bmatrix} \begin{Bmatrix} \bar{w} \\ \bar{v} \end{Bmatrix} + \begin{bmatrix} \boldsymbol{0}_{N\times 1} & \boldsymbol{0}_{N\times 1} \\ \boldsymbol{M}^{-1}\boldsymbol{B}_1 & -\boldsymbol{M}^{-1}\boldsymbol{K}_2\bar{w} \end{bmatrix} \begin{Bmatrix} V_1(t) \\ V_2(t) \end{Bmatrix} \tag{9}$$

III. Model Validation

Because the model of the structure is nonlinear, we opt to validate the model in its quasi-linear state by using linear system techniques. To validate this approach, a membrane strip made of Kapton is considered. Four MFC patches (M-2814-P1), made by Smart Materials Corporation, are used to construct the two bimorphs. The BBM is placed at $x_1 = 2.5$ cm, and the ABM is placed at $x_3 = 15.2$ cm (measured from the left boundary in Fig. 1). Table 1 shows the relevant physical properties of the structure.

A schematic of the experimental setup is shown in Fig. 2. The Kapton strip is held between two grippers. The left gripper remains fixed, and the right gripper can be translated to produce a tensile load in the structure. A MLP-75 load cell, made by Transducer Techniques, is used to measure the tension in the structure. A Polytec laser vibrometer (model OFV 303) is used to measure the velocity of a point on the centerline of the Kapton strip.

A burst chirp signal is supplied to the BBM to excite the structure in the transverse direction. The chirp signal had a peak amplitude of 0.1 V and a frequency range of 0.01–300 Hz. The excitation signal is amplified by a factor of 20 through a Trek amplifier (model 50/750). Siglab of Spectral Dynamics (model 20–42) is used to construct the frequency response of the structure. The uniform tension $\mathcal{T}$ is set to 16 N, and the measurement was taken at 9 cm from the left boundary. Two voltage values were supplied to the ABM: 75 and 150 V. The voltage value remained constant throughout the excitation period of the BBM. Figures 3a and 3b show the experimental and theoretical frequency responses of the structure with 0, 75, and 150 V applied to the ABM. Table 2 lists the values of the first two natural frequencies as obtained from the FEM model and from the experiment, along with the percentage errors. The percentage error is calculated according to

$$\text{error } \% = \frac{|f_{\text{exp}} - f_{\text{FEM}}|}{f_{\text{exp}}} \times 100$$

The FEM model presented predicts the first two frequencies within 3% error for the three cases tested.

IV. Control Law Design

The sliding mode technique is a variable-structure control technique in which the dynamics of a nonlinear system are altered via application of a high-frequency switching control [25,26]. This approach enables a robust control system in the presence of system uncertainties. In the following, two control problems are treated: 1) regulation and 2) reference tracking. For the regulation problem, it is desired to maintain the membrane strip at its undeformed configuration after a disturbance. On the other hand, when dealing with structures, it is more appropriate to refer to reference tracking as shape control. The control objective is to maintain the structure at a desired configuration.

A. System Uncertainties

The system expressed by Eq. (2) has been verified experimentally in its quasi-linear form [21]. Standard membrane mirror materials (e.g., Kapton and Mylar) are viscoelastic. Figure 4 shows the stress–strain behavior of a Kapton strip with the same dimensions as that tested in Sec. III. An Instron machine (model 4204) was used to

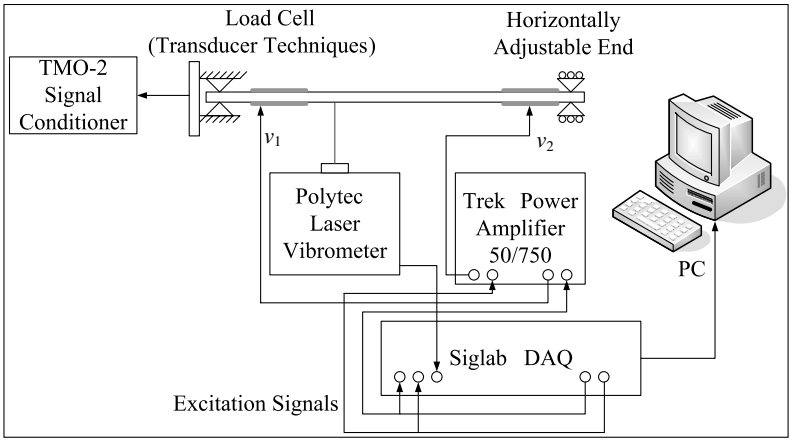

Fig. 2 Schematic of the experimental setup.

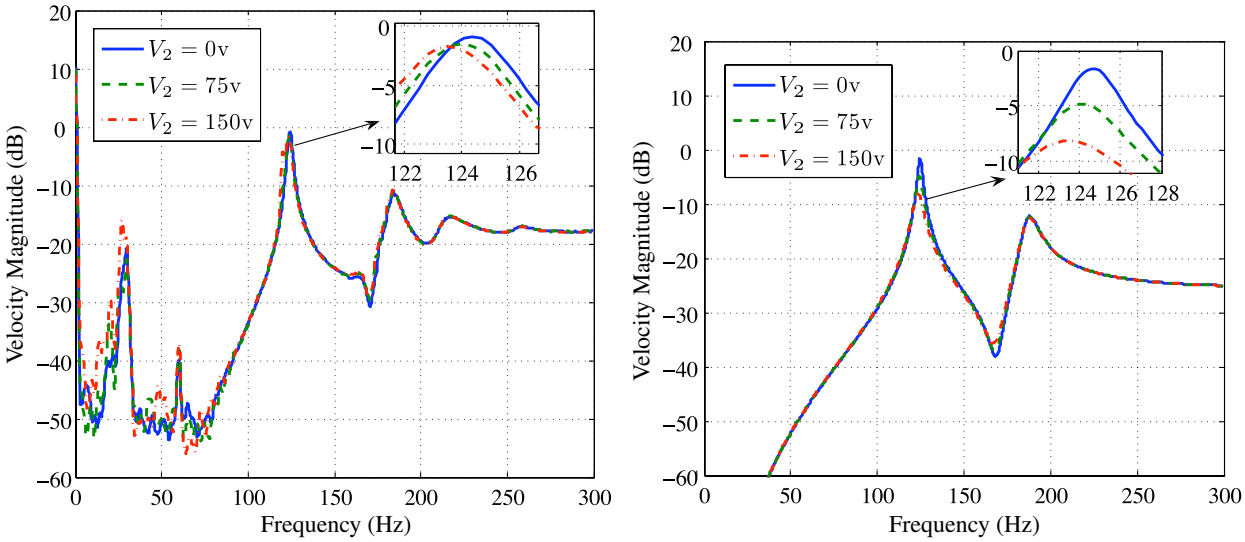

a) Experimental frequency response **b) FEM frequency response**

Fig. 3 Frequency response of the membrane mirror strip.

perform this test. The numerical bounds on the modulus of elasticity are obtained by calculating the maximum slope attained by the stress–strain curve of Fig. 4. Moreover, it is difficult to fully evaluate structural damping and air damping. In the following, the hat indicates the maximum value that can be attained by the variable. We assume that the membrane-strip modulus of elasticity and strain damping coefficient are such that

$$E_m \le \hat{E}_m \quad \text{and} \quad c_m \le \hat{c}_m$$

For the MFC patches, the bounds on the modulus of elasticity and the strain damping coefficient are

$$E_k \le \hat{E}_k \quad \text{and} \quad c_k \le \hat{c}_k \qquad (k = 1, 2)$$

Additionally, the air-damping coefficient can be bounded:

$$\gamma \le \hat{\gamma}$$

B. Controller Development

In this section, we derive the sliding mode controller. We outline the procedure without details. For in-depth discussions of the sliding mode technique, the reader is referred to Khalil [26].

Equation (9) can be cast into the standard form for applying the sliding mode control by defining the new variables:

$$\boldsymbol{\eta} = \bar{\boldsymbol{w}} \quad \text{and} \quad \boldsymbol{\xi} = \bar{\boldsymbol{v}}$$

In terms of the new variables, Eq. (9) can be written as

$$\dot{\boldsymbol{\eta}} = \boldsymbol{\xi}, \qquad \dot{\boldsymbol{\xi}} = \boldsymbol{f}_a(\boldsymbol{\eta}, \boldsymbol{\xi}) + \boldsymbol{G}_a(\boldsymbol{\eta}, \boldsymbol{\xi})\boldsymbol{u} + \boldsymbol{\delta}_\xi(\boldsymbol{\eta}, \boldsymbol{\xi}) \qquad (10)$$

where

Table 2 FEM vs experimental results

V_2, V	Frequency, Hz	FEM	Experiment	Error, %
0	f_1	125	124.5	0.40
	f_2	188	184	2.17
75	f_1	124	124.1	0.70
	f_2	186	182.7	1.81
150	f_1	123	123.5	0.40
	f_2	183	179.75	1.81

$$\begin{aligned}
\boldsymbol{f}_a(\boldsymbol{\eta}, \boldsymbol{\xi}) &= -\boldsymbol{M}^{-1}\bar{\boldsymbol{K}}_1\boldsymbol{\eta} - \boldsymbol{M}^{-1}\bar{\boldsymbol{C}}\boldsymbol{\xi} \\
\boldsymbol{G}_a(\boldsymbol{\eta}, \boldsymbol{\xi}) &= [\,\boldsymbol{M}^{-1}\boldsymbol{B}_1 \quad -\boldsymbol{M}^{-1}\boldsymbol{K}_2\boldsymbol{\eta}\,] \\
\boldsymbol{\delta}_\xi(\boldsymbol{\eta}, \boldsymbol{\xi}) &= \boldsymbol{M}^{-1}[(\bar{\boldsymbol{K}}_1 - \boldsymbol{K}_1)\boldsymbol{\eta} + (\bar{\boldsymbol{C}} - \boldsymbol{C})\boldsymbol{\xi}] \\
\boldsymbol{u} &= [\,V_1(t) \quad V_2(t)\,]^T
\end{aligned} \qquad (11)$$

where $\bar{\boldsymbol{K}}$ and $\bar{\boldsymbol{C}}$ are the nominal system matrices. The function $\boldsymbol{\delta}_\xi(\boldsymbol{\eta}, \boldsymbol{\xi})$ is a perturbation term that accounts for the difference between the nominal values and the actual values of the system matrices. Note that $\boldsymbol{G}_a(\boldsymbol{\eta}, \boldsymbol{\xi})$ is not square and that the $\boldsymbol{\eta}$ dynamics can be stabilized through an appropriate choice of $\boldsymbol{\xi}$. Let $\boldsymbol{\xi} = \boldsymbol{\phi}(\boldsymbol{\eta}) = -\alpha\boldsymbol{\eta}$ with $\alpha > 0$: a choice that would cause $\boldsymbol{\eta}$ to decay exponentially. To this end, define $\boldsymbol{z} = \boldsymbol{\xi} - \boldsymbol{\phi}(\boldsymbol{\eta})$. Using Eq. (10), the $\boldsymbol{z}$ dynamics can be described as

$$\dot{\boldsymbol{z}} = \boldsymbol{f}_a(\boldsymbol{\eta}, \boldsymbol{z}) + \boldsymbol{G}_a(\boldsymbol{\eta}, \boldsymbol{z})\boldsymbol{u} + \boldsymbol{\delta}_\xi(\boldsymbol{\eta}, \boldsymbol{z}) - \frac{\partial \boldsymbol{\phi}}{\partial \boldsymbol{\eta}}(\boldsymbol{z} + \boldsymbol{\phi}(\boldsymbol{\eta})) \qquad (12)$$

If $\boldsymbol{z}$ is driven to zero in finite time and maintained at zero, then $\boldsymbol{\xi}$ is driven to $\boldsymbol{\phi}(\boldsymbol{\eta})$. As a consequence, the $\boldsymbol{\eta}$ dynamics would evolve according to $\dot{\boldsymbol{\eta}} = \boldsymbol{\phi}(\boldsymbol{\eta}) = -\alpha\boldsymbol{\eta}$. Hence, the control input to drive $\boldsymbol{z}$ to zero (and maintain it at zero) is

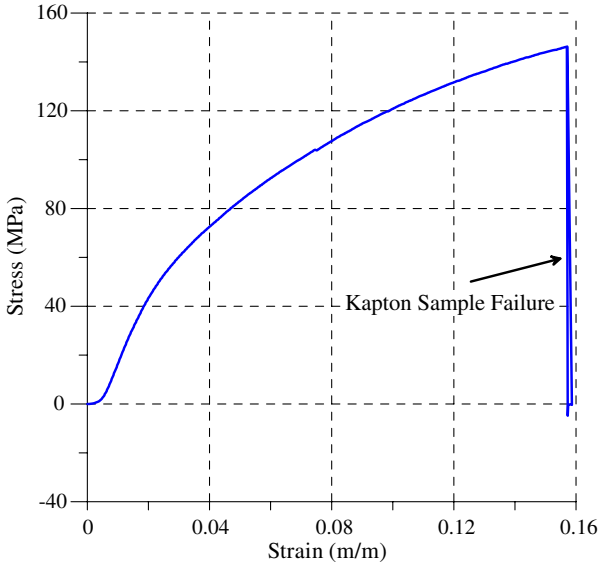

Fig. 4 Stress–strain curve of Kapton sample.

$$\boldsymbol{u} = \boldsymbol{u}_{\text{eq}} + \boldsymbol{G}_a^{+}(\eta, z)\boldsymbol{v} \tag{13}$$

where $\boldsymbol{v}$ is a new control input, and $\boldsymbol{u}_{\text{eq}}$ is the control input necessary to cancel the nominal dynamics of the system:

$$\boldsymbol{u}_{\text{eq}} = \boldsymbol{G}_a^{+}(\eta, z)\left[-\boldsymbol{f}_a(\eta, z) + \frac{\partial \boldsymbol{\phi}}{\partial \eta}(z + \boldsymbol{\phi}(\eta))\right]$$

where $\boldsymbol{G}_a^{+}(\eta, z)$ is the pseudoinverse of $\boldsymbol{G}_a(\eta, z)$, given as

$$\boldsymbol{G}_a^{+}(\eta, z) = \left[\boldsymbol{G}_a^{T}(\eta, z)\boldsymbol{G}_a(\eta, z)\right]^{-1}\boldsymbol{G}_a(\eta, z) \tag{14}$$

Substituting the control input of Eq. (13) in the dynamics of Eq. (12) yields

$$\dot{z} = \boldsymbol{v} + \boldsymbol{\delta}_{\xi}(\eta, z, \boldsymbol{u}) \tag{15}$$

The perturbation term $\boldsymbol{\delta}_{\xi}(\eta, z)$ can be bounded because the system matrices $\boldsymbol{K}_1$ and $\boldsymbol{C}$ are bounded matrices. Their nominal values are

$$\bar{\boldsymbol{K}}_1 = \left[\int_0^L (\overline{EI}(x)\phi_i''(x)\phi_j''(x) + \mathcal{T}\phi_i'(x)\phi_j'(x))\mathrm{d}x\right]_{(i,j=1,\ldots,N)}$$
$$\bar{\boldsymbol{C}} = \left[\int_0^L (\overline{cI}(x)\phi_i''(x)\phi_j''(x) + \overline{\gamma}\phi_i(x)\phi_j(x))\mathrm{d}x\right]_{(i,j=1,\ldots,N)} \tag{16}$$

where $\overline{EI}$, $\overline{cI}$, and $\bar{\gamma}$ are the nominal values of the flexural stiffness, structural damping, and air damping, respectively. When evaluating the norm of $\boldsymbol{\delta}_{\xi}(\eta, z)$, one can use the triangular inequality to obtain

$$\|\boldsymbol{\delta}_{\xi}(\eta, \xi)\| \le \|\boldsymbol{M}^{-1}\bar{\boldsymbol{K}}_1\eta\| + \|\boldsymbol{M}^{-1}\boldsymbol{K}_1\eta\| + \|\boldsymbol{M}^{-1}\bar{\boldsymbol{C}}\xi\| + \|\boldsymbol{M}^{-1}\boldsymbol{C}\xi\|$$

Recall that $\|\boldsymbol{A}\boldsymbol{x}\| \le \|\boldsymbol{A}\|_i\|\boldsymbol{x}\|$, where $\|.\|_i$ is the induced matrix norm on $\mathbb{R}^{N\times N}$ for $\boldsymbol{A} \in \mathbb{R}^{N\times N}$ (e.g., [27]). The perturbation term is further bounded as

$$\begin{aligned}\|\boldsymbol{\delta}_{\xi}(\eta, \xi)\| &\le \|\boldsymbol{M}^{-1}\bar{\boldsymbol{K}}_1\|_i\|\eta\| + \|\boldsymbol{M}^{-1}\boldsymbol{K}_1\|_i\|\eta\| \\ &\quad + \|\boldsymbol{M}^{-1}\bar{\boldsymbol{C}}\|_i\|\xi\| + \|\boldsymbol{M}^{-1}\boldsymbol{C}\|_i\|\xi\| \\ &\le \left(\frac{EI(x) + \max[EI(x)]}{\rho(x)}\right)\|\eta\| \\ &\quad + \left(\frac{cI(x) + \gamma + \max[cI(x) + \gamma]}{\rho(x)}\right)\|\xi\|\end{aligned} \tag{17}$$

The linear density, flexural stiffness, and structural damping are nonuniform, as expressed in the Appendix. The value of these properties reaches a maximum at the location of the bimorphs. Hence, define the function $\beta(\eta, \xi)$ to be

$$\begin{aligned}\beta(\eta, \xi) &= \left(\frac{\overline{EI}(x) + \max[EI(x)]}{\min[\rho(x)]}\right)\|\eta\| \\ &\quad + \left(\frac{\overline{cI}(x) + \overline{\gamma} + \max[cI(x) + \gamma]}{\min[\rho(x)]}\right)\|\xi\|\end{aligned} \tag{18}$$

where $\|\boldsymbol{\delta}_{\xi}(\eta, \xi)\| \le \beta(\eta, \xi)$. The maximum value of the flexural stiffness and damping can be calculated using the maximum values given in Sec. IV.A and the expressions of the Appendix. A proper choice of the new control input $\boldsymbol{v}$ is

$$\boldsymbol{v} = -\beta(\eta, \xi)\mathbf{sat}(z) = -\beta(\eta, \xi)\begin{Bmatrix}\mathrm{sat}(z_1)\\ \vdots \\ \mathrm{sat}(z_N)\end{Bmatrix} \tag{19}$$

where the saturation function is given by

$$\mathrm{sat}\,(z_1) = \begin{cases}\frac{z_1}{\epsilon} & \text{if } |\frac{z_1}{\epsilon}| \le 1\\ \mathrm{sign}(\frac{z_1}{\epsilon}) & \text{if } |\frac{z_1}{\epsilon}| > 1\end{cases} \quad \text{with } \epsilon > 0 \tag{20}$$

Note that the saturation function approaches the sign function as ϵ approaches zero. The use of the saturation function enables the control effort to smoothly approach zero. Hence, the control input becomes

$$\boldsymbol{u} = \boldsymbol{G}_a^{+}(\eta, \xi)\left[-\boldsymbol{f}_a(\eta, \xi) + \frac{\partial \boldsymbol{\phi}}{\partial \eta}\xi - \beta(\eta, \xi)\mathbf{sat}(\xi - \phi(\eta))\right]$$

In terms of the original state variables, the proposed control law is given as

$$\boldsymbol{u} = \boldsymbol{G}_a^{+}(\bar{\boldsymbol{w}}, \bar{\boldsymbol{v}})\left[-\boldsymbol{f}_a(\bar{\boldsymbol{w}}, \bar{\boldsymbol{v}}) + \frac{\partial \boldsymbol{\phi}}{\partial \bar{\boldsymbol{w}}}\bar{\boldsymbol{v}} - \beta(\bar{\boldsymbol{w}}, \bar{\boldsymbol{v}})\mathbf{sat}(\bar{\boldsymbol{v}} - \boldsymbol{\phi}(\bar{\boldsymbol{w}}))\right] \tag{21}$$

A quadratic Lyapunov function can be used to show that the derived control law stabilizes the system asymptotically.

C. System Singularities

Matrix $\boldsymbol{G}_a(\eta, \xi) = \boldsymbol{G}_a(\bar{\boldsymbol{w}}, \bar{\boldsymbol{v}})$ of Eq. (11) is a function of the deflection $\bar{\boldsymbol{w}}$. A singularity occurs when $\bar{\boldsymbol{w}} = 0$, because the second column of $\boldsymbol{G}_a(\bar{\boldsymbol{w}}, \bar{\boldsymbol{v}})$ will vanish, and hence $\boldsymbol{G}_a^{+}(\bar{\boldsymbol{w}}, \bar{\boldsymbol{v}})$ cannot be defined. This singularity is due to the ABM actuator. To alleviate this problem, a switching algorithm is proposed:

$$\boldsymbol{G}_a(\bar{\boldsymbol{w}}, \bar{\boldsymbol{v}}) = \begin{cases}[\,\boldsymbol{M}^{-1}\boldsymbol{B}_1 \quad -\boldsymbol{M}^{-1}\boldsymbol{K}_2\bar{w}\,] & \text{if } \mu[\boldsymbol{G}_a^{T}(\bar{\boldsymbol{w}}, \bar{\boldsymbol{v}})\boldsymbol{G}_a(\bar{\boldsymbol{w}}, \bar{\boldsymbol{v}})] < 10^{10}\epsilon_0\\ \boldsymbol{M}^{-1}\boldsymbol{B}_1 & \text{otherwise}\end{cases} \tag{22}$$

where $\mu(\boldsymbol{A})$ is the reciprocal condition estimator of $\boldsymbol{A} \in \mathbb{R}^{N\times N}$ and ϵ_0 is the distance from 1.0 to the next-larger double-precision number [28]. In other words, as the membrane strip approaches the original configuration, the effect of the axial force induced by the ABM diminishes. Fortunately, this switching command is not merely based on convenience. If the strip is undeformed, the ABM would have no effect on the transverse motion. Mathematically, this event coincides with the failure to calculate the pseudoinverse of $\boldsymbol{G}_a(\bar{\boldsymbol{w}}, \bar{\boldsymbol{v}})$.

As the switching between control algorithms is deployed, the closed-loop control system becomes a hybrid (continuous in time, discrete regarding the switching signal) control system. Switching can destabilize the system even if the individual subsystems are stable. However, in this case, the existence of a common quadratic Lyapunov function guarantees the stability of the hybrid closed-loop system [29].

D. Shape Control

This work focuses on a membrane strip as a prelude to studying a circular membrane augmented with smart actuators near its outer rim. The ultimate goal of this research is to be able to correct for optical aberrations of a circular membrane mirror using mechanical actuation via smart materials. To be able to do this, a means to translate an optical aberration into a mechanical presentation must be established. Ruggiero [18] showed that a mapping exists between the optical and mechanical realms. Optical aberrations are usually expressed in terms of Zernike polynomials. Ruggiero considered a circular lens. He expanded the Zernike polynomials into the mechanical mode shapes and concluded that optical aberrations up to the fifth order can be canceled through deforming the membrane mirror into an appropriate combination of the mechanical mode shapes. Extended discussion of Zernike polynomials, image aberrations, and correction approaches can be found in [30,31].

As this work treats a membrane strip augmented with smart actuators, the shape-control problem of this structure will be treated herein. Shape control of structures has attracted many researchers. Varadarajan et al. [32] presented an adaptive control law to perform shape control of laminated composite plates under quasi-statically-varying unknown loads. Sun and Tong [33] presented a design optimization of control voltage distribution for constrained static shape control of structures augmented with lead zirconate titanate (PZT) patches. Moreover, Sun and Tong [34] treated the local

shape-control problem. Their target was to control the shape of a part of a structure, rather than the entire structure, while minimizing the energy used to achieve the desired shape. Renno and Inman [35] presented a proportional–integral optimal controller for a membrane strip actuated using a single PZT bimorph. The shape-control problem considered in this paper treats a structure actuated by two bimorphs, BBM and ABM. Most of the previously published literature did not include an axial actuator.

To this end, let the desired shape (i.e., the desired transverse deformation) be $\bar{\boldsymbol{w}}_d = \boldsymbol{\eta}_d$ with a zero final velocity. Define the following error variables:

$$\boldsymbol{e}_1 = \boldsymbol{\eta} - \boldsymbol{\eta}_d \quad \text{and} \quad \boldsymbol{e}_2 = \boldsymbol{\xi} \tag{23}$$

The initial conditions of the new variables are $\boldsymbol{e}_1(0) = -\boldsymbol{\eta}_d$ and $\boldsymbol{e}_2(0) = \boldsymbol{\xi}(0) = \boldsymbol{0}$, because the structure starts from the undeformed static configuration $\boldsymbol{\eta}(0) = \boldsymbol{0}$. The error dynamics are given as

$$\dot{\boldsymbol{e}}_1 = \boldsymbol{e}_2, \qquad \dot{\boldsymbol{e}}_2 = \boldsymbol{f}_a(\boldsymbol{e}_1, \boldsymbol{e}_2) + \boldsymbol{G}_a(\boldsymbol{e}_1, \boldsymbol{e}_2)\boldsymbol{u} + \boldsymbol{\delta}_{\boldsymbol{e}_2}(\boldsymbol{e}_1, \boldsymbol{e}_2) \tag{24}$$

where

$$\boldsymbol{f}_a(\boldsymbol{e}_1, \boldsymbol{e}_2) = -\boldsymbol{M}^{-1}\bar{\boldsymbol{K}}_1(\boldsymbol{e}_1 + \boldsymbol{\eta}_d) - \boldsymbol{M}^{-1}\bar{\boldsymbol{C}}\boldsymbol{e}_2$$

$$\boldsymbol{G}_a(\boldsymbol{e}_1, \boldsymbol{e}_2) = [\,\boldsymbol{M}^{-1}\boldsymbol{B}_1 \quad -\boldsymbol{M}^{-1}\boldsymbol{K}_2(\boldsymbol{e}_1 + \boldsymbol{\eta}_d)\,]$$

$$\boldsymbol{\delta}_{\boldsymbol{e}_2}(\boldsymbol{e}_1, \boldsymbol{e}_2) = \boldsymbol{M}^{-1}[(\bar{\boldsymbol{K}}_1 - \boldsymbol{K}_1)(\boldsymbol{e}_1 + \boldsymbol{\eta}_d) + (\bar{\boldsymbol{C}} - \boldsymbol{C})\boldsymbol{e}_2]$$

The input vector $\boldsymbol{u}$ remains as defined in Eq. (11). The same procedure presented for the regulation problem is followed herein. The same function $\boldsymbol{e}_2 = \boldsymbol{\phi}(\boldsymbol{e}_1) = -\alpha\boldsymbol{e}_1$ with $\alpha > 0$ is used to stabilize the $\boldsymbol{e}_1$ subsystem. Then we introduce $\boldsymbol{z} = \boldsymbol{e}_2 - \boldsymbol{\phi}(\boldsymbol{e}_1)$ and develop the control law through bounding the perturbation term $\boldsymbol{\delta}_{\boldsymbol{e}_2}(\boldsymbol{e}_1, \boldsymbol{e}_2)$. For this case, the bounding function is given by

$$\beta(\boldsymbol{e}_1, \boldsymbol{e}_2) = \left(\frac{\overline{EI}(x) + \max[EI(x)]}{\min[\rho(x)]}\right)(\|\boldsymbol{e}_1\| + \|\boldsymbol{\eta}_d\|) + \left(\frac{\overline{cI}(x) + \overline{\gamma} + \max[cI(x) + \gamma]}{\min[\rho(x)]}\right)\|\boldsymbol{e}_2\| \tag{25}$$

and the resulting control input is

$$\boldsymbol{u} = \boldsymbol{G}_a^{+}(\boldsymbol{e}_1, \boldsymbol{e}_2)\left[-\boldsymbol{f}_a(\boldsymbol{e}_1, \boldsymbol{e}_2) + \frac{\partial\boldsymbol{\phi}}{\partial\boldsymbol{e}_1}\boldsymbol{e}_2 - \beta(\boldsymbol{e}_1, \boldsymbol{e}_2)\mathbf{sat}(\boldsymbol{e}_2 - \boldsymbol{\phi}(\boldsymbol{e}_2))\right] \tag{26}$$

The convergence of $\boldsymbol{e}_1$ and $\boldsymbol{e}_2$ to the origin yields the desired shape of the membrane strip. As in the regulation problem, a quadratic Lyapunov function can be used to prove asymptotic stability of the closed-loop system. Additionally, the same switching command is implemented for the shape-control problem: that is,

$$\boldsymbol{G}_a(\boldsymbol{e}_1, \boldsymbol{e}_2) = \begin{cases} [\,\boldsymbol{M}^{-1}\boldsymbol{B}_1 \quad -\boldsymbol{M}^{-1}\boldsymbol{K}_2(\boldsymbol{e}_1 + \boldsymbol{\eta}_d)\,] & \text{if } \mu[\boldsymbol{G}_a^T(\boldsymbol{e}_1, \boldsymbol{e}_2)\boldsymbol{G}_a(\boldsymbol{e}_1, \boldsymbol{e}_2)] < 10^{10}\epsilon_0 \\ \boldsymbol{M}^{-1}\boldsymbol{B}_1 & \text{otherwise} \end{cases} \tag{27}$$

where $\mu(\cdot)$ and ϵ_0 were defined in Sec. IV.C.

V. Case Study and Simulation

To demonstrate the efficacy of the controller, the structure presented in Sec. III is considered. The nominal properties of the specimen at hand are listed in Table 1. The bounds on the uncertain physical properties are

$$E \le 6 \text{ GPa}, \qquad c_m \le 45 \times 10^8 \text{ N}\cdot\text{s/m}^2, \qquad E_k \le 39 \text{ GPa},$$
$$c_k \le 45 \times 10^8 \text{ N}\cdot\text{s/m}^2 \qquad (k = 1, 2), \qquad \gamma \le 1 \text{ N}\cdot\text{s/m} \tag{28}$$

The bounding values of the uncertain parameters were obtained through comparison with the experimental results presented in [21]. The controller parameters used throughout this work are

$$\alpha = 30 \quad \text{and} \quad \epsilon = 10^{-4} \tag{29}$$

The following subsections present simulation examples for the regulation and shape-control problems.

A. Regulation Examples

Here, three cases are considered. In each case, the structure is disturbed using a forcing signal applied to the BBM for an appropriate period of time. Then the controller is activated to regulate the deformation of the structure.

1) In case I, the uniform tension $\mathcal{T}$ in the structure is set to 5 N. The linearized first natural frequency at this uniform tension value is 61 Hz. To excite the structure to the first mode shape, a sinusoidal voltage of amplitude 200 V and frequency of 61 Hz is applied to the BBM. This forcing signal is applied for 1.65 s, then the controller is activated.

2) For case II, the uniform tension $\mathcal{T}$ is set to 3 N. The linearized second natural frequency at this value of uniform tension is 74 Hz. The structure is excited through the BBM using a sinusoidal voltage of amplitude 200 V and frequency of 74 Hz. Similar to case I, the controller is activated after this period.

For case I and case II, the open-loop excitation time is nearly commensurate with the period of the structure, such that when the controller is activated, the structure would be deformed and moving away from the undeformed position.

3) Case III is considered to further demonstrate the effectiveness of the controller. The uniform tension $\mathcal{T}$ in the structure is set to 3 N. The forcing signal is the summation of three sinusoidal signals, each having an amplitude of 200 V. The frequencies are the first three linearized frequencies of the structure (47, 74, and 174 Hz). The forcing signal excites the structure for 1.5 s, after which the controller is activated. For this case, the duration of open-loop excitation is chosen arbitrarily.

Figure 5 shows the open-loop behavior of the membrane strip for case I and case II. The closed-loop response is shown in Fig. 6. The membrane strip returns back to its original undeformed configuration in a smooth fashion for both case I and case II. The control input is displayed in Fig. 7.

The results show an interesting behavior. It was demonstrated in [21], experimentally and theoretically, that positive values of $V_2(t)$ induce a softening effect in the structure. Positive voltage supplied to the ABM caused the natural frequencies of the structure to drop to lower values. Conversely, negative voltage values have a stiffening effect. For both case I and case II, at the end of the open-loop excitation, the structure is deformed and moving away from equilibrium. To bring the structure back to its undeformed shape, it is desired to stiffen the structure. This is demonstrated in Figs. 7a and 7b, in which $V_2(t)$ is negative. Moreover, as the maximum initial displacement of the structure increased, the value of $V_2(t)$ grew more negative. Figure 5a shows a maximum initial displacement of about 0.3 mm, and Fig. 5b shows a maximum initial displacement of about 0.5 mm. Recall that both case I and case II use the same amplitude for

the open-loop excitation but with different pretension levels. Case I targets the first mode shape, and case II targets the second mode shape. Moreover, Figs. 3a and 3b indicate that the deformation amplitude is higher at the first natural frequency. However, the uniform tension in case II is 3 N, which causes less stiffness in the structure and hence the higher amplitude observed in Fig. 5b.

Figure 8 shows the open-loop behavior of the structure for case III. Figure 8a displays the time history of the structure's deformation, and Fig. 8b displays the time history of the structure's deformation velocity. Again, in this case, the controller is able to suppress the strip's vibration, as shown in Fig. 9a. The control effort is displayed in Fig. 9b.

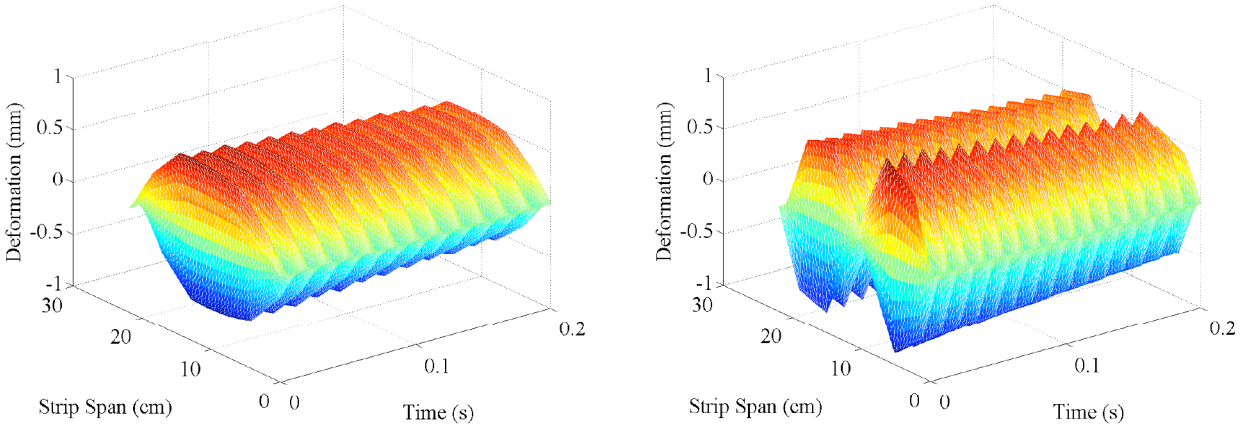

a) Case I **b) Case II**

Fig. 5 Time history of the deformation: open-loop response.

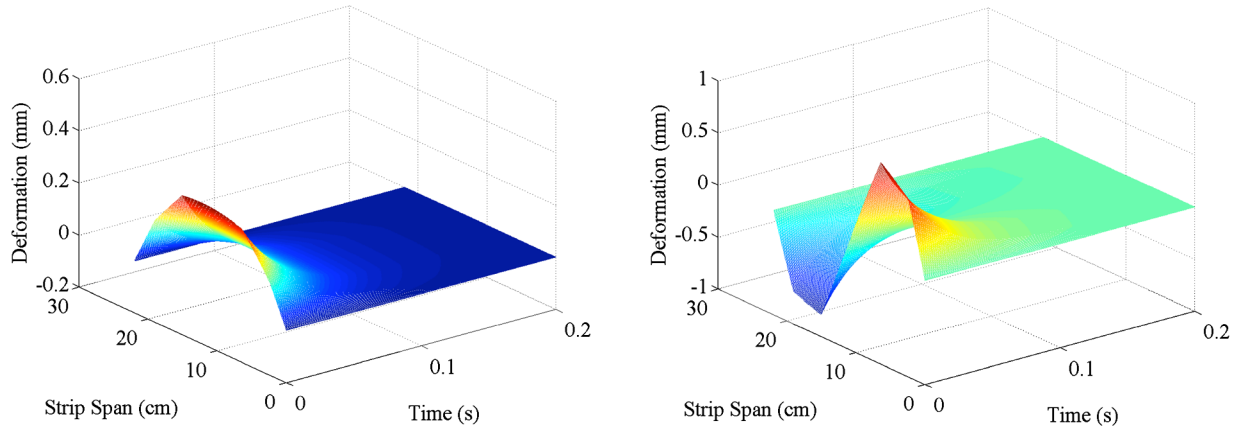

a) Case I **b) Case II**

Fig. 6 Time history of the deformation: closed-loop response.

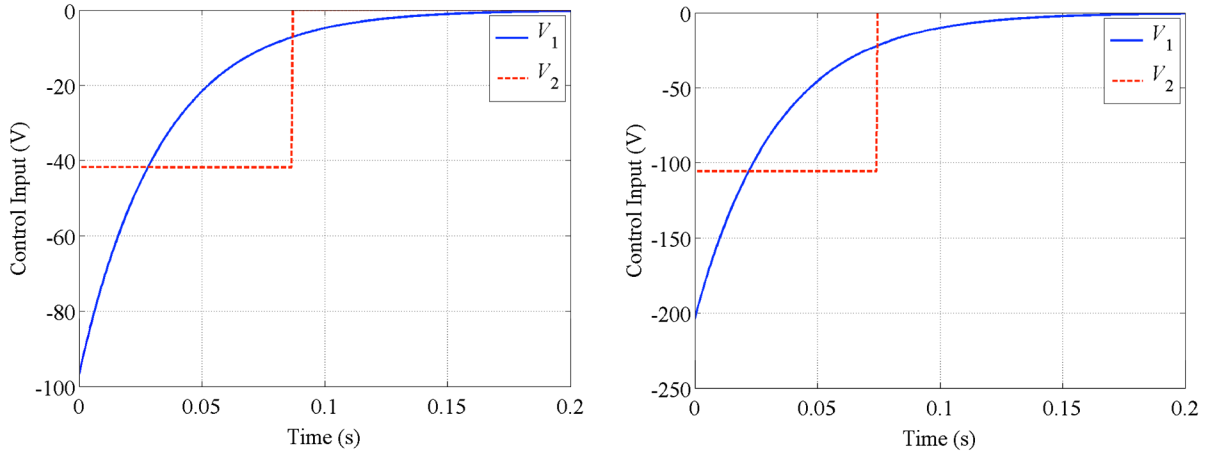

a) Case I **b) Case II**

Fig. 7 Time history of the control input.

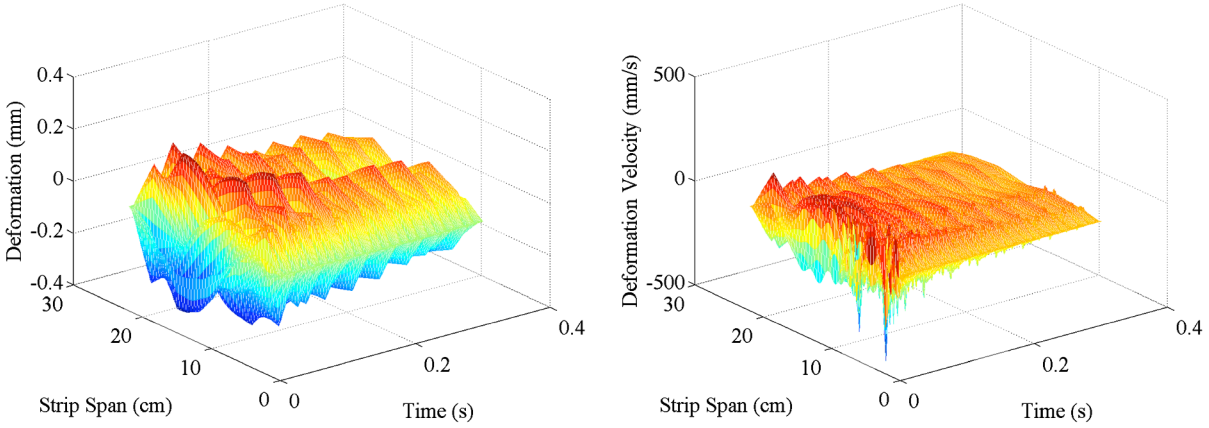

a) Time history of the deformation

b) Time history of the deformation velocity

Fig. 8 Open-loop behavior for case III.

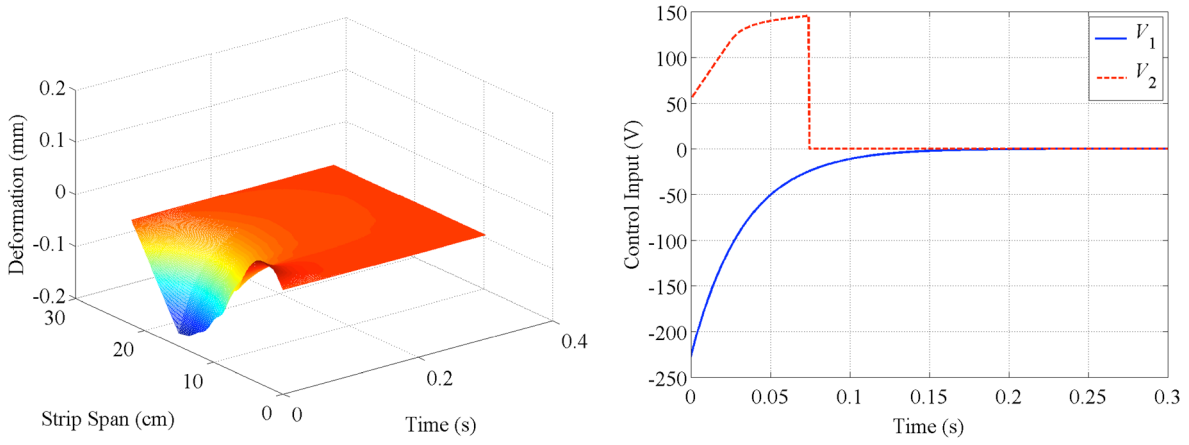

a) Time history of the deformation

b) Time history of the control input

Fig. 9 Closed-loop behavior for case III.

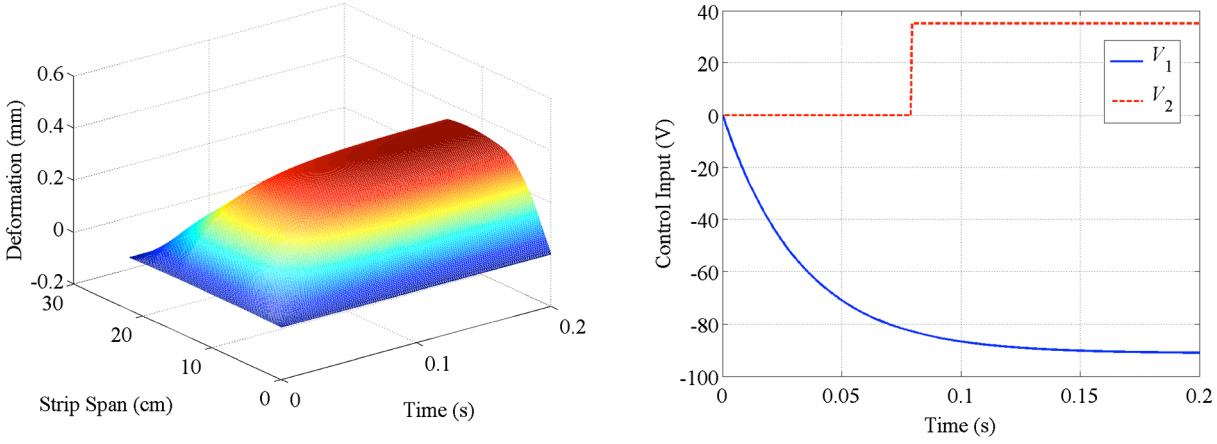

a) Time history of the deformation

b) Time history of the control input

Fig. 10 Closed-loop behavior of case IV.

B. Shape Control Examples

Now, instead of regulating the configuration of the membrane strip, it is desired to deform the membrane strip to a specified shape and hold it at this configuration. Two cases are presented here:

1) In case IV, the uniform tension is set to 5 N. It is desired to deform the membrane strip to its first mode shape, which can be attained through the open-loop excitation of case I. The corresponding maximum deformation of the structure is 0.34 mm.

2) In case V, the uniform tension is 3 N. The reference command is the first mode shape, which can be attained through an open-loop excitation of a sinusoidal signal of amplitude 200 V and frequency 47 Hz. The corresponding maximum deformation of the structure is 0.37 mm.

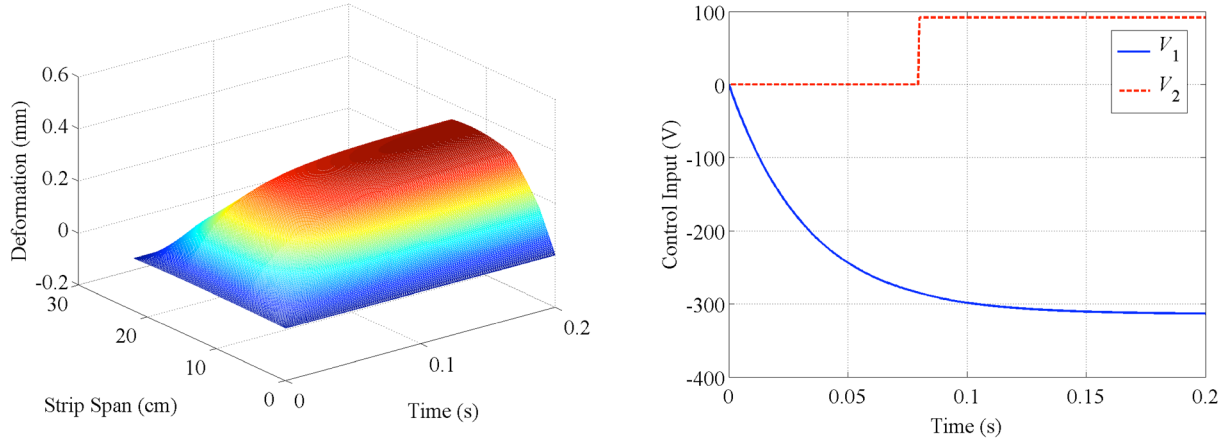

a) Time history of the deformation **b) Time history of the control input**

Fig. 11 Closed-loop behavior of case V.

For case IV, the time history of deformation of the membrane strip and the voltage applied to the BBM and ABM are shown in Figs. 10a and 10b, respectively. Figure 11a and 11b display the time history of the deformation and the voltage applied to the BBM and ABM for case V.

The results shown in Figs. 10 and 11 agree with the regulation examples presented previously. Recall that the purpose of case IV and case V is to deform the membrane strip. From elementary vibration, it is desirable to lower the stiffness of the structure to facilitate the deformation. This is particularly substantiated in Figs. 10b and 11b. The values of $V_2(t)$, the voltage applied to the ABM, are positive. According to the results presented in Sec. III and in [21], positive values of $V_2(t)$ induce a softening effect. It is also noted that the value of $V_2(t)$ for case IV is less than the value of V_2 for case V. This can be explained as follows. The maximum desired deformation in case IV is 0.34 mm, and the maximum desired deformation in case V is 0.37 mm. To achieve a larger deformation, a larger steady-state voltage value is required at the BBM. Moreover, a larger softening effect is required, hence the larger value of $V_2(t)$.

VI. Conclusions

In this paper, we treat the control problem of a membrane mirror strip actuated axially and in bending. The membrane mirror strip is modeled as an Euler–Bernoulli beam under tension. The axial bimorph induces a discontinuous tensile load in the structure, and hence the model of the system is nonlinear. We develop a sliding mode controller for regulation and shape-control problems. In regulation, the undeformed equilibrium is stabilized, whereas in shape control, a desired shape of the structure is achieved. The advantage of using the sliding mode technique is that it guarantees the stability of the system in the presence of system uncertainty. Traditionally, a bounding function is used to assure Lyapunov stability. Yet, the presence of the tension bimorph can cause closed-loop instability. Consequently, a switching command is used to avoid instability, which coincides with a structural singularity. The existence of a common Lyapunov function guarantees the stability of the switched system. Three regulation examples and two shape-control examples are presented. The results presented show that the controller has excellent stabilization and tracking properties.

Appendix

The linear density of the structure is

$$\rho(x) = \rho_m h_m b_m + \sum_{k=1}^{2} 2\rho_k h_k b_k \chi_k(x) \tag{A1}$$

The internal bending moment is given as

$$M_x(x,t) = EI(x)\frac{\partial^2 w(x,t)}{\partial x^2} + cI(x)\frac{\partial^3 w(x,t)}{\partial t \partial x^2}$$

where the flexural stiffness is

$$EI(x) = \frac{1}{12} b_m h_m^3 E_m + \sum_{k=1}^{2} \frac{2}{3} a_k b_k E_k \chi_k(x) \tag{A2}$$

and the Kelvin–Voigt damping is

$$cI(x) = \frac{1}{12} b_m h_m^3 c_m + \sum_{k=1}^{2} \frac{2}{3} c_k a_k b_k \chi_k(x) \tag{A3}$$

Here, the function $\chi_k(x)$ is given as

$$\chi_k(x) = \begin{cases} 1 & \text{if } x_{2k-1} \le x \le x_{2k} \\ 0 & \text{otherwise} \end{cases} \tag{A4}$$

The bending constant of the kth bimorph is

$$(\kappa_B)_k = -\tfrac{1}{2} E_k b_k (h_m + h_k)(d_{31})_k \tag{A5}$$

and the axial constant is

$$(\kappa_A)_k = -E_k b_k (d_{31})_k \tag{A6}$$

Acknowledgments

Funding for this work is administered by the Center of Intelligent Material Systems and Structures on behalf of the U.S. Air Force Office of Scientific Research under grant FA9550-06-1-0143. The authors wish to thank Dan K. Marker of the Advanced Optics and Imaging Division at the U.S. Air Force Research Lab for motivating this work. The authors appreciate the fruitful discussions and valuable suggestions of Eric J. Ruggiero of the Performance Technologies Laboratory at GE Global Research Center.

References

[1] Cassapakis C., and Thomas M., "Inflatable Structures Technology Development Overview," AIAA 1995 Space Programs and Technologies Conference, AIAA Paper 1995-3738, Sept. 1995.

[2] Ruggiero, E., Jha, A., Park, G., and Inman, D., "A Literature Review of Ultra-Light and Inflated Toroidal Satellite Components," *The Shock and Vibration Digest*, Vol. 35, No. 3, May 2003, pp. 171–181. doi:10.1177/0583102403035003001

[3] Ruggiero, E., Jacobs, J., and Babb, B., "A SPIDER Technology Overview," AIAA/ASME/ASCE/AHS/ASC Structures, Structural

Dynamics, and Material Conference, AIAA Paper 2004-1822, Apr. 2004.
[4] Ruggiero, E., and Inman, D., "Gossamer Spacecraft: Recent Trends in Design, Analysis Experimentation and Control," *Journal of Spacecraft and Rockets*, Vol. 43, No. 1, Jan. 2006, pp. 10–24. doi:10.2514/1.8232
[5] Jenkins, C. (ed.), *Gossamer Spacecraft: Membrane and Inflatable Structures Technology for Space Applications*, Progress in Astronautics and Aeronautics, Vol. 191, AIAA, Reston, VA, 2001.
[6] Jenkins, C. (ed.), *Recent Advances in Gossamer Spacecraft*, Progress in Astronautics and Aeronautics, Vol. 212, AIAA, Reston, VA, 2006.
[7] Gorinevsky, D., and Hyde, T., "Adaptive Membrane for Large Lightweight Space Telescopes," *Highly Innovative Space Telescope Concepts*, Proceedings of SPIE: The International Society for Optical Engineering, Vol. 4849, Society of Photo-Optical Instrumentation Engineers, Bellingham, WA, 2002, pp. 330–338.
[8] Bales, G., Hall, J., Flint, E., and Glaese, R., "Experimental Issues that Impact in Vacuum Dynamic Characterization of Thin Film Membranes," AIAA/ASME/ASCE/AHS/ASC Structures, Structural Dynamics, and Material Conference, AIAA Paper 2003-1743, Apr. 2003.
[9] Young, L., and Pai, P., "Numerical and Experimental Dynamic Characteristics of Thin-Film Membranes," AIAA/ASME/ASCE/AHS/ASC Structures, Structural Dynamics, and Material Conference, AIAA Paper 2004-1618, Apr. 2004.
[10] Pollard, E., deBlonk, B., Erwin, R., and Jenkins, C., "Characterizing the Non-Linear Behavior of Membrane Optics," *Space Systems Engineering and Optical Alignment Mechanisms*, Proceedings of SPIE: The International Society for Optical Engineering, Vol. 5528, Society of Photo-Optical Instrumentation Engineers, Bellingham, WA, 2004.
[11] Moore, J., Patrick, B., Chodimella, S., Marker, D., and deBlonk, B., "Design and Testing of a One-Meter Membrane Mirror with Active Boundary Control," *UV/Optical/IR Space Telescopes: Innovative Technologies and Concepts 2*, Proceedings of SPIE: The International Society for Optical Engineering, Vol. 5899, Society of Photo-Optical Instrumentation Engineers, Bellingham, WA, 2005.
[12] Marker, D., and Jenkins, C., "Surface Precision of Optical Membrane with Curvature," *Optics Express*, Vol. 1, No. 11, 1997, pp. 324–331.
[13] Chodimella, S., Moore, J., and Patrick, B., "Design, Fabrication and Validation of an Ultra-Lightweight Membrane Mirror," *Advanced Wavefront Control: Methods, Devices, and Applications 3*, Proceedings of SPIE: The International Society for Optical Engineering, Vol. 5894, Society of Photo-Optical Instrumentation Engineers, Bellingham, WA, 2005.
[14] Marker, D., Rotge, J., Carreras R., Duneman, D., and Wilkes, J., "Minimum Strain Requirements for Optical Membranes," *High-Resolution Wavefront Control: Methods, Devices and Applications*, Proceedings of SPIE: The International Society for Optical Engineering, Society of Photo-Optical Instrumentation Engineers, Bellingham, WA, July 1999, pp. 224–231.
[15] Wilkes, J., Jenkins, C., Marker, D., Carreras R., Duneman, D., and Rotge, J., "Concave Membrane Mirrors from Aspheric to Near Parabolic," *High-Resolution Wavefront Control: Methods, Devices and Applications*, Society of Photo-Optical Instrumentation Engineers, Bellingham, WA, July 1999, pp. 213–223.
[16] Shepherd, M., Peterson, G., Cobb, R., and Palazotto, A., "Quasi-Static Optical Control of In-Plane Actuated, Deformable Mirror: Experimental Comparison with Finite Element Analysis," AIAA/ASME/ASCE/AHS/ASC Structures, Structural Dynamics, and Material Conference, AIAA Paper 2006-2231, May 2006.
[17] Shepherd, M., Cobb, R., and Baker, W., "Clear Aperture Design Criterion for Deformable Membrane Mirror Control," *IEEE Aerospace Conference*, Inst. of Electrical and Electronics Engineers, Piscataway, NJ, May 2006. doi:10.1109/AERO.2006.1655889
[18] Ruggiero, E., "Modeling and Control of SPIDER Satellite Components," Ph.D. Dissertation, Dept. of Mechanical Engineering, Virginia Polytechnic Inst. and State Univ., Blacksburg, VA, July 2005.
[19] Wilkie, W., Bryant, R., High, J., Fox, R., Hellbaum, R., Jalink, A., Little, B., and Mirick, P., "Low-Cost Piezocomposite Actuator for Structural Control Application," *Smart Structures and Materials 2000*, Society of Photo-Optical Instrumentation Engineers, Bellingham, WA, Mar. 2000, pp. 323–334.
[20] Renno, J., Tarazaga, P., Seigler, M., and Inman, D., "Modeling of a Membrane Mirror Actuated Using Piezoelectric Bimorph," ASME International Mechanical Engineering Congress and Exposition (IMECE2006), American Society of Mechanical Engineers Paper IMECE2006-13224, Nov. 2006.
[21] Renno, J., and Inman, D., "An Experimentally Validated Model of a Membrane Mirror Strip Actuated Using Multiple Active Fiber Composites for Adaptive Optics," *Journal of Spacecraft and Rockets*, Vol. 44, No. 5, 2007, pp. 1140–1152. doi:10.2514/1.27843
[22] Prenter, P., *Splines and Variational Methods*, Wiley, New York, 1975.
[23] deBoor, C., Hollig, K., and Riemenschneider, S., *Box Splines*, Applied Mathematical Sciences, Vol. 98, Springer–Verlag, New York, 1992.
[24] Hollig, K., *Finite Element Methods with B-Splines: Frontiers in Applied Mathematics*, Society for Industrial and Applied Mathematics, Philadelphia, 2001.
[25] Utkin, V., *Sliding Modes in Control and Optimization*, Springer–Verlag, New York, 1992.
[26] Khalil, H., *Nonlinear Systems*, 3rd ed., Prentice–Hall, Upper Saddle River, NJ, 2000.
[27] Vidyasagar, M., *Nonlinear Systems Analysis Classics in Applied Mathematics*, 2nd ed., Society for Industrial and Applied Mathematics, Philadelphia, 1993.
[28] Anderson, E., Bai, Z., Bishof, C., Blackford, S., Demmel, J., Dongarra, J., Du Croz, J., Greenbaum, A., Hammarling, S., McKenny, A., and Sorensen, D., *LAPACK Users' Guide*, 3rd ed., Society for Industrial and Applied Mathematics, Philadelphia, 1999.
[29] Liberzon, D., *Switching in Systems and Control, Systems & Control: Foundation & Applications*, Birkhäuser, Boston, 2003.
[30] Malacara, D., *Optical Shop Testing, Pure and Applied Optics*, 2nd ed., Wiley, New York, 1992.
[31] Tyson, R. K., *Introduction to Adaptive Optics*, SPIE Tutorial Texts in Optical Engineering, Vol. TT41, Society of Photo-Optical Instrumentation Engineers, Bellingham, WA, Mar. 2000.
[32] Varadarajan, S., Chandrashkhara, K., and Agarwal, S., "Adaptive Shape Control of Laminated Composite Plates Using Piezoelectric Materials," *AIAA Journal*, Vol. 36, No. 9, Sept. 1998, pp. 1694–1698. doi:10.2514/2.573
[33] Sun, D., and Tong, L., "Optimum Control Voltage Design for Constrained Static Shape Control of Piezoelectric Structures," *AIAA Journal*, Vol. 41, No. 12, Dec. 2003, pp. 2444–2450. doi:10.2514/2.6843
[34] Sun, D., and Tong, L., "Energy Optimization in Local Shape Control of Structures with Nonlinear Piezoelectric Actuators," *AIAA Journal*, Vol. 43, No. 10, Oct. 2005, pp. 2210–2217. doi:10.2514/1.7649
[35] Renno, J., and Inman, D., "Modeling and Control of Membrane Mirror Strip Using Single Piezoelectric Bimorph," *Journal of Vibration and Control*, e-First Publication Jan. 2009. doi:10.1177/1077546308088563

C. Cesnik
Associate Editor